Quaternary Science Reviews 122 (2015) 222–232

Contents lists available at ScienceDirect

Quaternary Science Reviews

journal homepage: www.elsevier.com/locate/quascirev

Changes in biomass burning mark the onset of an ENSO-influenced climate regime at 42°S in southwest Tasmania, Australia

Michael-Shawn Fletcher [a, b, *], Alexa Benson [a], Hendrik Heijnis [c], Patricia S. Gadd [c], Les C. Cwynar [d], Andrew B.H. Rees [d, e]

[a] School of Geography, University of Melbourne, Parkville, VIC, 3010, Australia
[b] Institute of Ecology and Biodiversity, University of Chile, Santiago, Chile
[c] Institute for Environmental Research, Australian Nuclear Science and Technology Organisation, Locked Bag 2001, Kirrawee DC, NSW, 2232, Australia
[d] Department of Biology, University of New Brunswick, Fredericton, New Brunswick, E3B 5A3, Canada
[e] School of Geography, Environment and Earth Sciences, Victoria University of Wellington, Wellington, 6012, New Zealand

ARTICLE INFO

Article history:
Received 19 February 2015
Received in revised form
1 May 2015
Accepted 5 May 2015
Available online 15 June 2015

Keywords:
El Niño-Southern Oscillation (ENSO)
Southern hemisphere westerly winds (SWW)
Tasmania
Southern Hemisphere
Fire
Geochemistry
Climate
Holocene

ABSTRACT

We use macroscopic charcoal and sediment geochemistry analysis of two proximal upper montane lakes located at 42°S in southwest Tasmania, Australia, to test the role of the southern hemisphere westerly winds (SWW) and the El Niño-Southern Oscillation (ENSO) in governing the climate of this sector of the southern mid-to high-latitudes. Inter-annual climate anomalies in the study area are driven by changes in both ENSO and the Southern Annular Mode (SAM - an index that describes seasonal to decadal shifts in the SWW), making it an ideal location to test assumptions about the varying influence of the SWW and ENSO, two important components of the global climate system, through time. We find multi-millennial scale trends in fire activity that are remarkably consistent with trends in hydroclimate reconstructed at the same latitude in southern South America, providing empirical support for the notion of zonally symmetric changes in the SWW governing the climate at this latitude in the Southern Hemisphere between 12 and 5 cal ka BP. A transition from multi-millennial scale to sub-millennial scale trends in fire activity occurs after ca 5 cal ka BP in concert with the onset of high frequency and amplitude ENSO variability in the tropical Pacific Ocean region. We conclude that the onset of sub-millennial scale trends in ENSO drove changes in fire activity in our study region over the last ca 5 cal ka. Geochemical data reveals divergent local impacts at the two study sites in response to these major climate transitions that are related to local topography and geography.

1. Introduction

El Niño activity, the warm phase of the El Niño-Southern Oscillation (ENSO), is projected to amplify as global temperatures rise, heralding a serious threat to water security and fire risk in areas located within the ENSO climate domain (Cook et al., 2004; Murphy and Timbal, 2008; Power et al., 2013). For example, El Niño events starve southeast Australia of rainfall, potentially resulting in drought and wildfire (Verdon et al., 2004; Nicholls and Lucas, 2007; Hill et al., 2009). The strength and frequency of El Niño events have varied considerably over the last 12,000 years (Moy et al., 2002; Riedinger et al., 2002; Conroy et al., 2008). The last few millennia, in particular, are characterised by a range of ENSO variability, significantly exceeding that of the historical period (Moy et al., 2002). Considering modern climate relationships, this implies the droughts, floods and wildfires associated with ENSO in the Pacific realm during recorded history might have been exceeded over the last few millennia. While some have speculated (albeit convincingly) that the marked increase in the frequency and amplitude of El Niño events after ca 6000 calendar years before present (6 cal ka BP: BP = 1950 CE) in the tropical Pacific Ocean drove widespread hydroclimatic change across the ENSO domain (McGlone et al., 1992; Shulmeister and Lees, 1995; Rodbell et al., 1999; Shulmeister, 1999; Fletcher and Moreno, 2011, 2012a), few studies present data of sufficient resolution to directly test the relationship between an amplified ENSO system and hydroclimate, particularly in the Australian sector of the southwest Pacific Ocean.

* Corresponding author. School of Geography, University of Melbourne, Parkville, VIC, 3010, Australia.
E-mail address: michael.fletcher@unimelb.edu.au (M.-S. Fletcher).

http://dx.doi.org/10.1016/j.quascirev.2015.05.002
0277-3791/

Indeed, we are aware of only one other study that is critically located and sufficiently resolved and to test this relationship (Rees et al., submitted for publication). Here, we use sediment charcoal, sediment geochemistry and radiometric analyses to reconstruct, and constrain temporally, long-term fire activity and catchment dynamics in extra-tropical Tasmania, Australia, over the last 12,000 years. We principally focus on the role of changing ENSO activity in the tropical Pacific Ocean region in driving changes in fire regimes and, by extension, climate in this cool temperate region.

An increase in the frequency of El Niño events in the tropical Pacific Ocean region is reported after ca 6–5 cal ka BP (Moy et al., 2002), with the effects of this amplification subsequently propagating into parts of the mid-to high-latitudes (the extra-tropics) of the South Pacific Ocean region (McGlone et al., 1992; Shulmeister and Lees, 1995; Rodbell et al., 1999; Shulmeister, 1999; Fletcher and Moreno, 2012a). Prior to this, the effects of ENSO in this area are thought to have been muted or absent, particularly in areas where changes in the strength and position of the southern westerly winds (SWW) govern the contemporary climate (Fletcher and Moreno, 2012a). A transition from climate regime dominated by multi-millennial scale trends in the SWW to a climate regime in which ENSO variability drives sub-millennial scale hydroclimatic variability occurs in parts of the mid-to high-latitudes of the South Pacific Ocean region after ca 6–5 cal ka BP and is observable in trends in trans-Pacific Ocean reconstructions of terrestrial hydroclimate and fire-regimes (Fletcher and Moreno, 2011, 2012a; Rees et al., submitted for publication). This transition is marked by a shift from a multi-millennial scale and zonally symmetric pattern of hydroclimate variation during the SWW-dominant phase prior to ca 6–5 cal ka BP to a sub-millennial scale zonally asymmetric pattern of hydroclimate variation during the succeeding ENSO-dominant period in areas under the influence of ENSO (Fletcher and Moreno, 2011, 2012a; Rees et al., submitted for publication).

Here we employ analyses of sedimentary charcoal, geochemistry and radiometric dating of two lakes located at 42°S in southwest Tasmania, Australia. Tasmania is a cool temperate island that falls under the influence of both ENSO and the Southern Annular Mode (SAM – an index that describes seasonal to decadal shifts in the position and intensity of the SWW). Shifts in the position and intensity of the SWW drive supra-annual precipitation and moisture anomalies in Tasmania: positive (negative) phases of the SAM result in negative (positive) precipitation and temperature anomalies, principally in the west of Tasmania where the SWW are intercepted by the north–south trending ranges that bisect the island (Hill et al., 2009). Indeed, this pattern occurs across the extra-tropics of the entire Southern Hemisphere (Garreaud, 2007), with 42°S representing the latitude of strongest correlation between SAM and rainfall anomalies on all southern landmasses (Gillett et al., 2006). In terms of ENSO, the El Niño (La Niña) phase of ENSO is associated with negative (positive) moisture anomalies across Tasmania, particularly in the north (Hill et al., 2009), while the opposite is true across most of the southeast Pacific Basin (Garreaud et al., 2009).

Fire in vegetation landscapes like Tasmania, which are uniformly wet and have a high vegetation biomass, are climate-limited – i.e., fuel is always abundant, but it must be sufficiently dry to burn (McWethy et al., 2013). Thus, temporal changes in charcoal deposition (read: biomass burning) in these regions is confined to anomalously dry periods (i.e., charcoal records are a good proxy for changes in hydroclimate) (Moreno, 2000; Whitlock et al., 2007; Fletcher and Moreno, 2012a). Further, fires destabilise landscapes, often resulting in post-fire erosion and nutrient loss (which we term here: catchment dynamics), with changes in fire regimes driving changes in catchment dynamics through time (Fletcher et al., 2014a). In this paper, we specifically ask: What drives changes in long-term fire activity in southwest Tasmania? Is there a relationship between the hypothesized millennial-scale trends in the SWW and fire activity in southwest Tasmania? Is there a relationship between the onset of amplified sub-millennial ENSO variability in the tropical Pacific Ocean region and fire regimes in southwest Tasmania? How do long-term changes in biomass burning influence the delivery and character of sediment delivery in to lakes from their surrounding catchment?

2. Southwest Tasmania

Tasmania (41–44° S) is a cool temperate continental island that is bisected by northwest–southeast trending mountain ranges that intercept mid-latitude cool and moisture laden SWW, resulting in a steep west–east orographic precipitation gradient. Temperatures are cool (5–7 °C in winter and 14–16 °C in summer) and precipitation (between 1200 and 3500 mm yr^{-1} annually) exceeds evaporation for most of the year (Gentilli, 1972; Sturman and Tapper, 2006). While the climate of the southwest, windward side of Tasmania is largely uniform throughout the year, seasonal migration of the SWW and associated storm tracks results in mild seasonal variation in rainfall. Longer-term shifts in the position and intensity of the SWW have a significant impact on Tasmanian climate (Gillett et al., 2006; Garreaud, 2007; Hill et al., 2009; Fletcher and Moreno, 2012a), with inter-annual precipitation and moisture anomalies significantly correlated with the SAM over the historic period: positive (negative) SAM results in negative (positive) rainfall anomalies in southwest Tasmania, particularly in spring and summer (Sept–Feb) (Hill et al., 2009). Supra-annual precipitation anomalies in Tasmania are also associated with tropical ENSO variability (Hill et al., 2009; Fletcher and Moreno, 2012a), with El Niño (La Niña) associated with negative (positive) precipitation anomalies in southwest Tasmania.

The topography of southwest Tasmania is rugged and complex, with a geological basement overwhelmingly composed of low-nutrient-yielding quartz-dominated metasediments (Jackson, 1999). The cool, wet climate and low bedrock nutrient status results in extreme oligotrophy that reduces primary productivity and results in remarkably slow rates of change in the vegetation of the region (Bowman and Jackson, 1981). Fire is an important ecological agent in southwest Tasmania (Jackson, 1968; Wood and Bowman, 2012) and human occupation for the past 40,000 years has had a major impact on the vegetation landscape (Bowman, 1998; Cosgrove, 1999; Bowman and Wood, 2009; Thomas et al., 2010; Fletcher and Thomas, 2010a; Fletcher et al., 2014a, 2014b). Treeless pyrophytic vegetation types dominate the landscape (including species of *Melaleuca*, *Leptospermum* and *Restionaceae* and *Gymnoschoenus sphaerocephalus*) and pyrophobic arboreal communities (rainforest) are restricted by topography and aspect and the protection those afford from fire (Wood et al., 2011). Montane and alpine communities are likewise characterised by fire-adapted and fire-sensitive types (Harris and Kitchener, 2005).

3. Materials and methods

3.1. Study sites

The two study sites are underlain by quartzite bedrock and are located on the north- and west-facing flanks of the imposing Frenchman's Cap massif (*Mabarlek* in the local indigenous language), in southwest Tasmania, Australia (Fig. 1). Frenchman's Cap (1445 masl) is a quartzite (Precambrian) peak that tops a broad and complex massif that rises sharply from the surrounding lowlands. Numerous glacial valleys and rock ledges host lakes on the massif. Areas on the exposed windward (north, west and south) flanks of

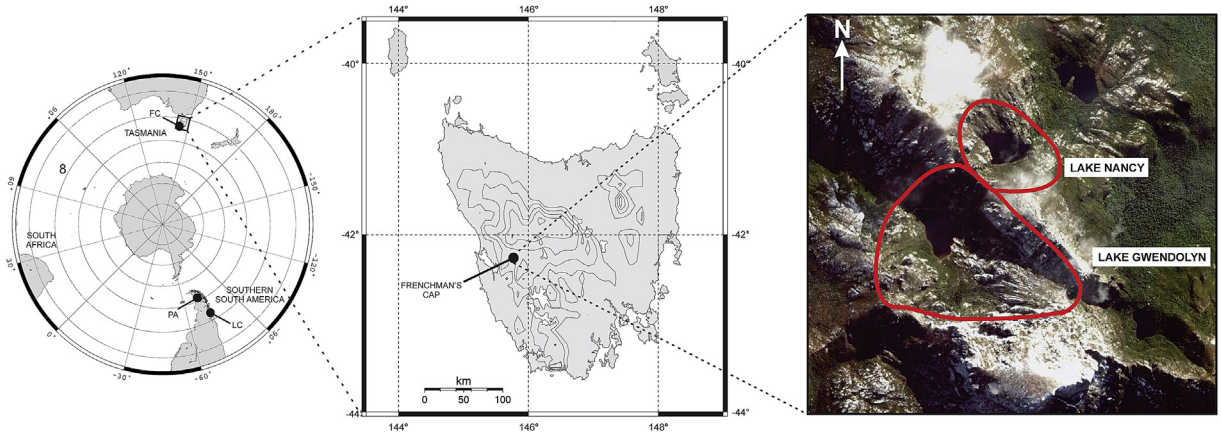

Fig. 1. A map of the study area showing the location of Tasmania in relation to other Southern Hemisphere landmasses, the location of Frenchman's Cap in Tasmania and the local setting and catchments of the study lakes. FC – Frenchman's Cap, Tasmania, Australia (this study). LC – Lago Condorito, Chile (Moreno, 2004). Laguna Potrok Aike, Argentina (Lisé-Pronovost et al., 2015).

the massif characterised by fire affected vegetation, whereas those on the lee side of the massif and in protected locations are vegetated by pyrophobic rainforest. Average annual rainfall at Butlers Gorge climate station (42.28°S, 146.28°E; 667 masl; 36 km east of our study lakes) is 1674.5 mm yr^{-1} and the temperature regime is cool (5–7 °C June to August; 14–16 °C December to February). Snow and ice are frequent on the summit of Frenchman's Cap in winter and at elevations above 900 masl.

3.1.1. Lake Gwendolyn (TAS1106)

Lake Gwendolyn (42°15′45.10″S; 145°49′23.55″E; 929 masl) is a moraine-bound lake that lies within a steep-sided northwest oriented glacial valley below the summit of Frenchman's Cap (Fig. 1). The lake has a surface area of 3.8 ha and a catchment of 108.7 ha. Maximum water depth is 30 m. The catchment soils at the western end of the lake are skeletal with considerable exposed rock in the catchment; while deeper soils at the headwall of the valley support a species poor scrub rainforest vegetation (*Athrotaxis selaginoides*, *Eucryphia milliganii*, *Nothofagus cunninghamii* and *Richea pandanifolia*). Elsewhere in the catchment, the vegetation displays the clear effects of repeated burning and is characterised by a range of species, including: *Richea sprengelioides*, *Leptospermum* spp., *Eucalyptus vernicosa Bauera rubioides*, *Astelia alpina*, *Agastachys odorata* and *Tasmannia lanceolata*.

3.1.2. Lake Nancy (TAS1107)

Lake Nancy (42°15′31.17″S; 145°49′38.47″E; 1041 masl) is a small steep-sided bedrock controlled lake basin located on the northeast face of a ridge that runs northwest from the summit of Frenchman's Cap (Fig. 1). Lake Nancy has a surface area of 2.7 ha and a catchment of 11.9 ha. Maximum water depth is 24.10 m. The vegetation of the Lake Nancy catchment also displays the effects of repeated burning. Presently, deep and steep gullies that drain into the southern end of Lake Nancy are protected from fires fanned by the dominant westerly flow and host areas of *A. selaginoides* and *Nothofagus gunnii* rainforest thickets. More exposed areas within the catchment to the north of the lake are comprised of fire affected vegetation and regenerating rainforest species (including: *Richea scoparia*, *A. alpina*, *T. lanceolata*, *R. sprengelioides*, *N. cunninghamii*, *E. vernicosa* and *B. rubioides*). The dwarf conifer *Diselma archeri* is common along the lake's shore.

3.2. Core collection and sampling

Sediment cores containing the undisturbed water–sediment interface were extracted from the lakes using a 6.8-cm diameter polycarbonate chamber attached to a Universal Gravity Corer (http://www.aquaticresearch.com) operated from a floating platform rigged from two pack rafts. The sediments were measured and stored in their original sampling tubes for transport to the laboratory, where they were split using a Geotek core splitter (Geotek, Daventry, UK). Half of the core was selected for destructive analyses, while the other half was reserved for scanning and archiving.

3.3. Chronology

Ten samples were selected from the uppermost 9 cm of each core to develop a recent chronology. Approximately 1.0 g dry weight samples were analysed from 0.5 cm thick samples for ^{210}Pb activity using α-spectroscopy at MyCore Scientific Incorporated (Dunrobin, Ontario, Canada) (Appleby and Oldfield, 1978; Binford, 1990). Sediment rates and ages were determined using the Constant Rate of Supply model (Appleby and Oldfield, 1978; Appleby, 2001). Three radiocarbon samples were analysed from Lake Gwendolyn and 4 from Lake Nancy at the DirectAMS Radiocarbon Dating Service laboratory (Bothell, Washington, United States). Sample thickness of all radiocarbon samples was 0.5 cm. The radiocarbon dates were calibrated to cal ka BP (BP = 1950 CE) using the Southern Hemisphere calibration curve (Hogg et al., 2013). An age–depth model was constructed for each site using the clam package for the software R (Blaauw and Christen, 2011; R Core Development Team, 2013).

3.4. Macroscopic charcoal

Continuous sediment subsamples of 1.25 cc from 0.5 cm intervals were processed for 'macroscopic' charcoal content (>125 μm) using standard procedures (Whitlock and Larsen, 2001). Carbonised particles were sieved with a 125 μm sieve and subsequently counted under a stereomicroscope. This data provides basic changes in charcoal delivery to a lake from within a source area of 3 km (Whitlock and Larsen, 2001). Time-series analysis of the charcoal data was performed using CharAnalysis (Higuera et al., 2009), which interpolates the charcoal data into evenly spaced time steps to allow time-series analyses.

CharAnalysis calculates a background charcoal ($CHAR_{back}$) component that is used to identify significant charcoal peaks that are assumed to reflect local fire events. $CHAR_{back}$ was calculated using a lowess smoother (1000 year) robust to outliers, and charcoal peaks were identified using a 2000 year window (Fig. 2h). Importantly, $CHAR_{back}$, is driven by fuel type changes, taphonomic processes of charcoal deposition and changes in the amount of biomass burning in a landscape (Clark and Royall, 1996; Whitlock and Larsen, 2001). In high altitude lakes with small catchments, such as our study lakes (particularly Lake Nancy), where the small catchment size minimises the influence of catchment storage and re-deposition of charcoal, $CHAR_{back}$ likely reflects biomass burning outside of the local catchment: i.e. extra-local biomass burning (Clark and Royall, 1996; Whitlock and Larsen, 2001). A combined CHAR curve was created for both lakes by interpolating each CHAR record to 80-year time steps (the lowest median accumulation rate of the sites) and summing CHAR z-scores from each site that were calculated from a pre-European CHAR average (12–0.2 cal ka) for each site.

3.5. Geochemistry

Geochemical data was obtained at the Australian Nuclear Science and Technology Organisation (ANSTO) laboratory (Lucas Heights, NSW, Australia) using a multi-function X-ray fluorescence (ITRAX) core scanner. The ITRAX core scanner produced 1-mm interval (for Lake Gwendolyn) and 0.5-mm interval (for Lake Nancy), non-destructive elemental analyses of the surface of the split cores. The ITRAX scans were performed using a molybdenum (Mo) tube set at 55 kV and 30 mA with a dwell time of 10 s. Following the primary analysis, principal component analysis (PCA) was performed with the geochemical dataset to ascertain the principal trend through the geochemical dataset. No data modification was performed prior to the PCA. The PCA was performed using PC-Ord for Windows version 4.27 (McCune and Mefford, 1999). Ratios of incoherent and coherent scattering measurements (Mo Inc/Coh) produced by the core scanner were used to determine the average atomic number of material in the sediment, which is a proxy for organic matter content (e.g.Burnett et al., 2011). Organic carbon has

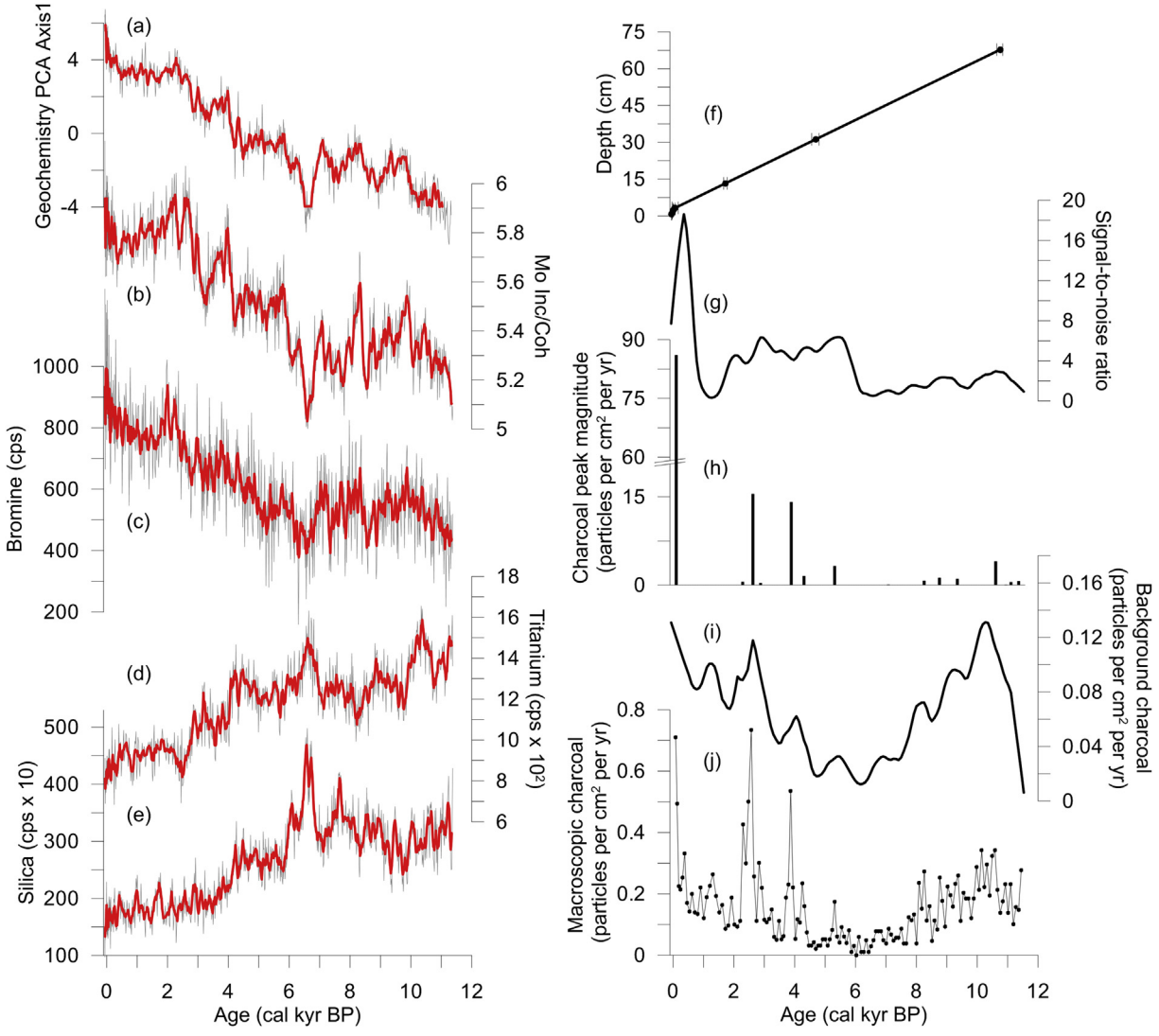

Fig. 2. A plot of geochemical, radiometric and charcoal data from Lake Gwendolyn (TAS1106) showing: (a) Geochemistry PCA axis 1; (b) Mo Inc/Coh scatter; (c) Bromine; (d) Titanium; (e) Silica; (f) smooth-spline age–depth model produced by clam (Blaauw, 2010) with 2-sigma errors on dates shown; (g) the signal-to-noise ratio produced by CharAnalysis (Higuera et al., 2009); (h) Background macroscopic CHAR ($CHAR_{back}$) produced by CharAnalysis (Higuera et al., 2009); and (i) macroscopic charcoal accumulation rates (CHAR).

Table 1
Table showing the results of the ^{210}Pb-total analysis of sediment cores from Lake Gwendolyn (TAS1106) and Lake Nancy (TAS1107), southwest Tasmania. The calculated ages are based on the constant rate of supply model.

Depth (cm)	^{210}Pb (total) (Bq g^{-1})	Age (cal. yr BP)	Error (years)	1s error
Lake Gwendolyn (TAS1106)				
0.0–0.5	0.182	2014	0	3.6
0.5–1.0	0.092	1989	4	3.7
1.0–1.5	0.084	1974	7	3.7
1.5–2.0	0.063	1955	26	4.1
2.0–2.5	0.065	1945	26	4
2.5–3.0	0.06	1926	66	5.2
3.0–3.5	0.059	1907	74	4
4.0–4.5	0.054	n/a	n/a	4.4
6.0–6.5	0.054	n/a	n/a	5
8.0–8.5	0.051	n/a	n/a	5.4
Lake Nancy (TAS1107)				
0.0–0.5	0.161	2014	0	3.3
0.5–1.0	0.113	1998	2	4.9
1.0–1.5	0.09	1981	4	4.8
1.5–2.0	0.054	1959	10	5
2.0–2.5	0.055	1945	12	5.1
2.5–3.0	0.041	1914	37	5.9
3.0–3.5	0.037	1880	99	7
4.0–4.5	0.031	n/a	n/a	7.5
6.0–6.5	0.031	n/a	n/a	8.9
8.0–8.5	0.033	n/a	n/a	7.4

a lower average atomic mass than other sedimentary material (eg. carbonate, aluminosilicates and silica): i.e. Mo Inc/Coh increases with greater concentrations of organic carbon. Indeed, comparisons between sediment organic carbon content and Mo Inc/Coh scattering reveal a strong positive relationship in a range of sedimentary environments (Saez et al., 2009; Burnett et al., 2011; Liu et al., 2013; Gadd et al., in press), validating the use of this proxy for sediment organic matter content. Further, bromine (Br) has been found to be a reliable proxy for organic matter content in both lacustrine and oceanic sediments (Phedorin et al., 2000; Croudace et al., 2006; Ziegler et al., 2008; Hahn et al., 2014) and Br content is significantly higher in organosols (the dominant soil type in southwest Tasmania) than in other soil types (Maw and Kempton, 1982), thus, providing an additional proxy for sediment organic matter content.

4. Results

4.1. Core collection and sampling

A continuous 71 cm core was collected from Lake Gwendolyn (TAS1106) from a lake depth of depth of 28.2 m, while a continuous 72 cm core was collected from Lake Nancy (TAS1107) from a lake depth of 24.1 m.

4.2. Chronology

4.2.1. Lake Gwendolyn (TAS1106)

Radiometric analyses were performed on the core, with ^{210}Pb dates displayed in Table 1. The lowest three samples (4.0, 6.0 and 8.0 cm) contained insufficient amounts of ^{210}Pb for dating. The lowest three samples contain supported ^{210}Pb only, as demonstrated by constant low values for total ^{210}Pb and therefore cannot (were not used) be used in the age calculation. The sequence of radiocarbon dates for Lake Gwendolyn were in stratigraphic order throughout the core and a maximum radiocarbon age of 9570 ^{14}C yrs BP was obtained at a depth of 67.5 cm (Table 2). The age–depth model (Fig. 2e) is based on a locally smoothed spline regression and is remarkably linear. The sediment accumulation rates remain consistent throughout the entirety of the core, with exception to the uppermost 200 years, where sedimentation rates increase.

4.2.2. Lake Nancy (TAS1107)

^{210}Pb dates obtained from Lake Nancy are displayed in Table 1. Again, the lowest three samples (4.0, 6.0 and 8.0 cm) did not contain sufficient ^{210}Pb for dating and therefore cannot be (and were not) used in the age calculation. The sequence of radiocarbon dates for Lake Nancy were in stratigraphic order throughout the core and a maximum radiocarbon age of 9840 ^{14}C yrs was obtained at a depth of 70.5 cm (Table 2). The age–depth model (Fig. 3e) is based on a locally smoothed spline regression and displays a trend of increasing sedimentation with depth. The sediment accumulation rates display a steady decrease in sedimentation rates from ca 11 cal ka BP to present until the uppermost section of the core, where sedimentation rates increase in the last 200 years.

4.3. Macroscopic charcoal

The combined CHAR record (Fig. 4d) shows multi-millennial changes in combined CHAR between ca 12 and 5 cal ka BP (characterised by increasing values to ca 11 cal ka BP, decreasing CHAR values toward a minima between 7 and 6 cal ka BP) and overall increasing CHAR values characterised by sub-millennial variation from ca 5 cal ka BP to the present.

4.3.1. Lake Gwendolyn (TAS1106)

Fourteen statistically significant peaks were identified through CharAnalysis (Fig. 2) (Higuera et al., 2010). An increase in charcoal peak magnitude is noted from ca 6 cal ka BP to present (Fig. 2g), while smaller magnitude peaks occur between ca12 and 6 cal ka BP. Macroscopic charcoal accumulations (CHAR) exhibit low frequency variability between ca 12 and 6 cal ka BP (Fig. 2i). Lowest CHAR values are recorded at ca 6 cal ka BP, increasing toward the present and displaying a higher frequency variability, with four notable large CHAR increases (0.25, 0.55, 0.75 and 0.71 particles cm^{-2} yr^{-1}, respectively). The average CHAR accumulation rate throughout the

Table 2
Radiocarbon dating results for TAS1106 and TAS1107. Calibrations (ca cal yr BP) are based on the Southern Hemisphere calibration curve, SHCal13 (Hogg et al., 2013).

Depth (cm)	Adjusted midpoint depth (cm)	Lab number	Material dated	Radiocarbon age (^{14}C yr BP)	Error (^{14}C yr BP)	δ^{13}C	Median age (cal ka BP)
Lake Gwendolyn (TAS1106)							
13.0–13.5	13.25	D-AMS 006301	Bulk sediment	1880	23	−20.8	1.787
31.0–31.5	31.25	D-AMS 006302	Bulk sediment	4249	30	−21.6	4.727
67.5–68.0	67.75	D-AMS 006303	Bulk sediment	9531	39	−40.8	10.775
Lake Nancy (TAS1107)							
12.5–13.0	12.75	D-AMS 006297	Bulk sediment	2029	27	−23	1.985
24.5–25.0	24.75	D-AMS 006298	Bulk sediment	4619	34	−32.9	5.219
50.0–50.5	50.25	D-AMS 006299	Bulk sediment	8306	38	−26.6	9.311
70.5–71.0	70.75	D-AMS 006300	Bulk sediment	9801	38	−30.6	11.159

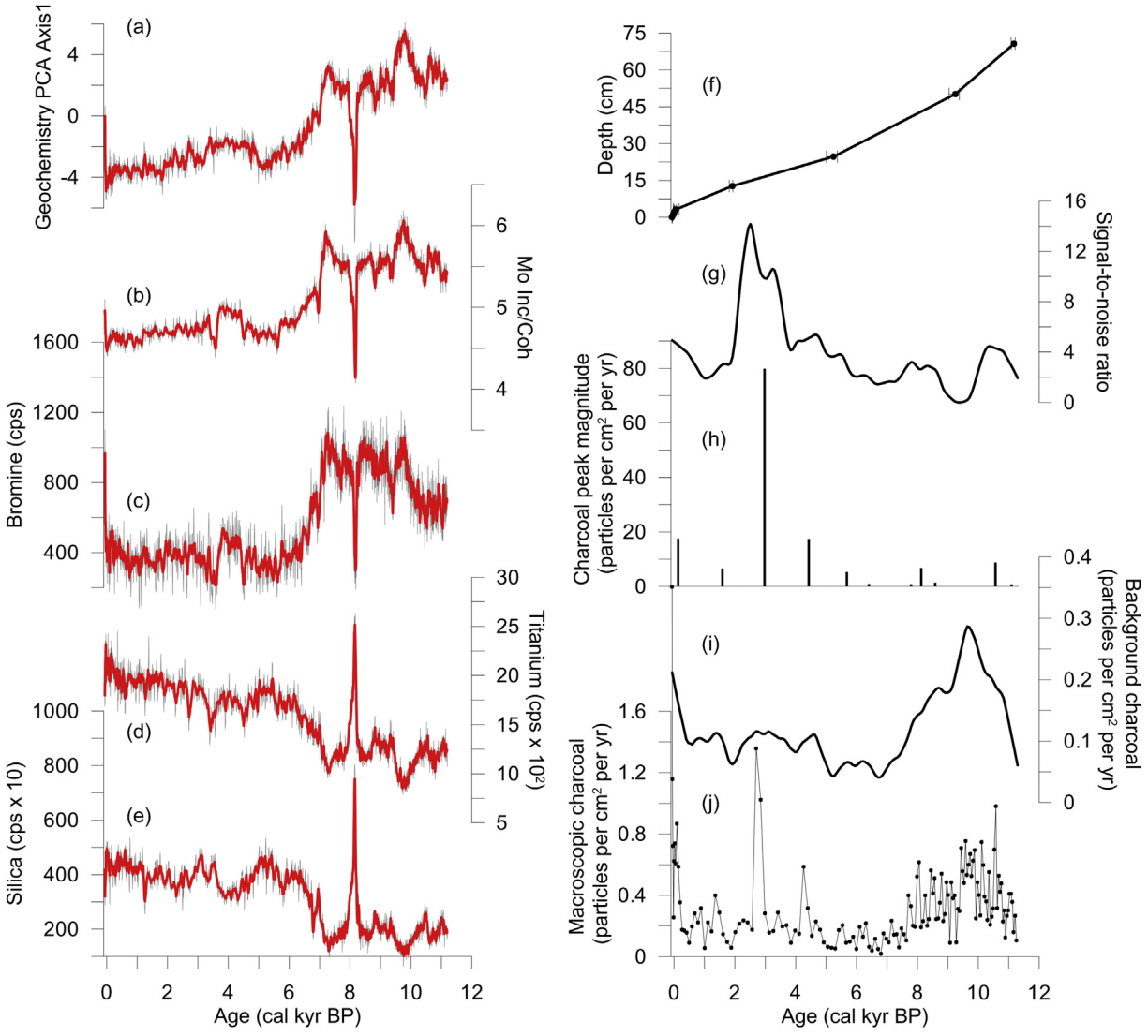

Fig. 3. A plot of geochemical, radiometric and charcoal data from Lake Nancy (TAS1107) showing: (a) Geochemistry PCA axis 1; (b) Mo Inc/Coh scatter; (c) Bromine; (d) Titanium; (e) Silica; (f) smooth-spline age–depth model produced by clam (Blaauw, 2010) with 2-sigma errors on dates shown; (g) the signal-to-noise ratio produced by CharAnalysis (Higuera et al., 2009); (h) Background macroscopic CHAR ($CHAR_{back}$) produced by CharAnalysis (Higuera et al., 2009); and (i) macroscopic charcoal accumulation rates (CHAR).

sequence is 0.15 particles cm^{-2} yr^{-1}. The signal-to-noise ratio is close to 3 throughout (Fig. 2f), indicating some statistical confidence in CHAR peak detection (Higuera et al., 2010).

4.3.2. Lake Nancy (TAS1107)

Twelve significant charcoal peaks were identified through CharAnalysis (Fig. 3g) (Higuera et al., 2010), the largest of which (80 particles cm^{-2} yr^{-1}) occurring at ca 2.7 cal ka BP. CHAR values are high and display low frequency variability between ca 12–7.5 cal ka BP (Fig. 3i). The average CHAR value is 0.3 particles cm^{-2} yr^{-1}. The signal-to-noise ratio is close to 3 throughout (Fig. 2f), indicating some statistical confidence in CHAR peak detection (Higuera et al., 2010).

4.4. Geochemistry

4.4.1. Lake Gwendolyn (TAS1106)

Detrital elements (Fe, K, Rb, Si, Sr, Ti, Zr), display strong, negative correlation with PCA axis 1, while Bromine (Br) displays a strong positive correlation with this axis (see Table 3). PCA axis 1 displays an overall increase in values from ca 12 cal ka BP to the present, with a marked increase occurring after ca 6.3 cal ka BP (Fig. 2).

4.4.2. Lake Nancy (TAS1107)

Detrital elements (K, Rb, Si, Ti, Zr) display a strong, negative correlation to the PCA data (see Table 3), whereas Br is positively correlated to this axis. PCA Axis 1 (Fig. 3) displays relatively steady (albeit variable) values between ca 12 and 7 cal ka BP, with a marked decrease from ca 7 cal ka to the present. A notable and short lived trend in the geochemical data occurs at ca 8.2 cal ka BP, with a marked increase in detrital elements and a dip in Br (Fig. 3).

5. Discussion

5.1. Millennial-scale climate

Our results reveal clearly synchronous changes in fire activity between our two study lakes at 42°S in Tasmania, Australia, throughout the last 12,000 years (Figs. 2–4). Because fire activity in this cool temperate region is limited by climate and its impact on

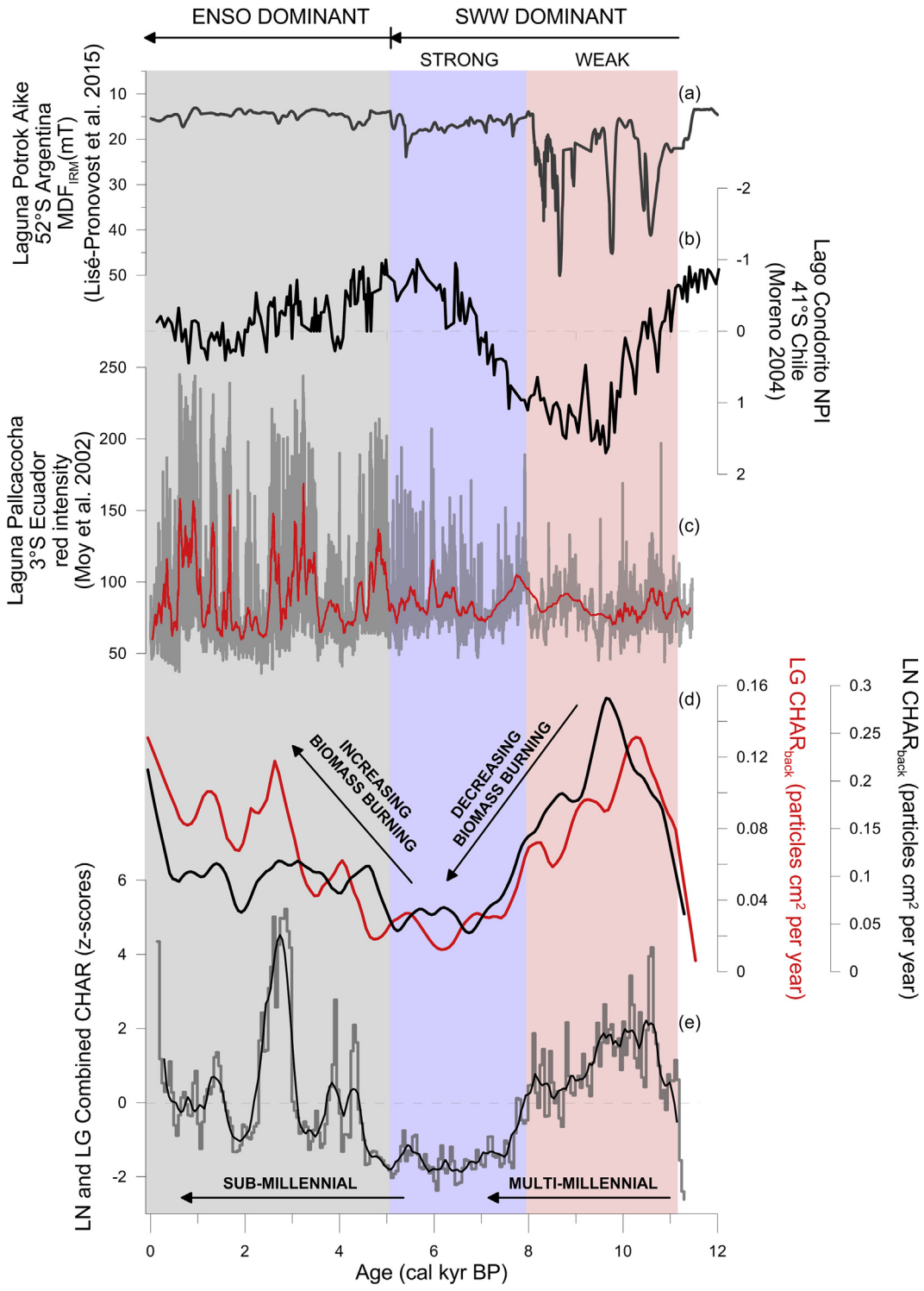

Fig. 4. A summary plot showing (a) Laguna Potrok Aike wind intensity proxy; (b) the Lago Condorito, Chile, North Patagonian Index (NPI – a semi-quantitative hydroclimate index based on selected pollen types) (Moreno, 2004); (c) Laguna Pallcacocha, Ecuador, red intensity data smoothed with a 59-point weighted averaging regression (a proxy for El Niño-driven erosion events (Moy et al., 2002); (d) trends in background CHAR (CHAR$_{back}$ – 1000-year smoothing window) at both Lake Gwendolyn (LG: red) and Lake Nancy (LN: black); and (e) combined CHAR records from both lakes (each CHAR record was interpolated to equal 80-year time-steps using CharAnalysis (Higuera et al., 2009) and z-scores were calculated from an average of pre-European (12–0.2 cal ka BP) CHAR values (smoothed with a 9-point weighted averaging regression). (For interpretation of the references to colour in this figure legend, the reader is referred to the web version of this article.)

the condition of the abundant fuel in this landscape (McWethy et al., 2013), it is possible to infer changes in hydroclimate from regional trends in fire activity (Fletcher and Moreno, 2012a). High and relatively uniform fire activity (inferred from CHAR$_{back}$) at both study sites between ca 11 and 8 cal ka BP implies a prolonged (multi-millennial) period of low relative moisture in the study region. Precipitation in this region is derived from the moisture-laden SWW as they rise over the Tasmanian landmass and expunge their moisture content (Gentilli, 1972). Indeed, the SWW are the dominant control over the climate of the mid-to high-latitudes of the

Table 3
Significant (>0.5 R^2) correlations and direction of correlation between geochemical data and the geochemical PCA axis 1.

Element	R^2	Direction
Lake Gwendolyn (TAS1106)		
K	0.936	−
Ti	0.78	−
Rb	0.743	−
Si	0.74	−
Zr	0.662	−
Fe	0.645	−
Br	0.599	+
Sr	0.599	−
Lake Nancy (TAS1107)		
Si	0.877	−
K	0.877	−
Ti	0.876	−
Zr	0.86	−
Rb	0.813	−
Br	0.619	+

entire Southern Hemisphere (SH) at scales ranging from daily to multi-millennial (Garreaud, 2007; Hill et al., 2009; Fletcher and Moreno, 2012a). Reductions in the intensity of SWW flow over 42°S in southwest Tasmania (i.e. SAM) are correlated with significant moisture deficits at this latitude over the historic period (Gillett et al., 2006). Moreover, 41–42°S marks the zone of strongest correlation between changes in the strength of the SWW and precipitation anomalies across the entire SH over the historic period (Gillett et al., 2006), implying that sites located in this critical latitude are highly sensitive to changes in the SWW.

Our identified period of increased fire activity between 11 and 8 cal ka BP is entirely consistent with a prolonged period of decreased SWW flow over the study region. Importantly, the increase in fire activity at our sites is synchronous with multi-millennial scale hydroclimatic trends identified at Lago Condorito at 41°S in Chile (Fig. 4b) (Moreno, 2004). The tight coupling between multi-millennial hydroclimatic change at sites located at 41–42°S almost 10,000 km apart mirrors the contemporary relationship between positive SAM and hydroclimate across the SH, implying a hemisphere-wide reduction in SWW flow over sites located at 41–42°S between ca 11 and 8 cal ka BP. Moreover, this phase of hemisphere-wide attenuated SWW flow over 41–42°S is synchronous with a reduction in wind intensity (derived from rock magnetic properties) at 52°S in Argentina (Lisé-Pronovost et al., 2015) (Fig. 4a), a location close to the modern SWW core (ca 50°S). Fletcher and Moreno (2011, 2012a) argue that the period between ca 11 and 8 cal ka BP in the mid-to high-latitudes of the SH was characterised by a phase of attenuated SWW flow over sites located above 50°S (the modern core of the SWW). This reduction in SWW flow is manifest as a reduction in SWW derived moisture on west-facing slopes and increased effective moisture on the lee side of the orographic barriers that bisect southern South America, New Zealand, Tasmania and, to a lesser extent, Southern Africa (Whitlock et al., 2007; Lamy et al., 2010; Fletcher and Moreno, 2011, 2012a; Kilian and Lamy, 2012), and this trend is entirely consistent with the results presented here. Similarly, the reduction in biomass burning recorded at our sites between ca 7 and 5 cal ka BP is synchronous with a prolonged period of increased moisture at Lago Condorito in Chile, and a hemisphere-wide trend toward strengthened SWW flow at sites located above 50°S (Moreno, 2004; Lamy et al., 2010; Fletcher and Moreno, 2011, 2012a; Lisé-Pronovost et al., 2015), adding significant weight to the notion of zonally symmetric changes in the SWW governing the climate at this latitude between 12 and 5 cal ka BP (sensu Fletcher and Moreno, 2012a).

5.2. The 8.2 cal ka event?

Of note is a thin band of inorganic sediment that was deposited in Lake Nancy at ca 8.2 cal ka BP (8.3–7.9 cal ka BP; 95% confidence interval) in concert with a charcoal peak of moderate magnitude (Fig. 3). A concomitant charcoal peak occurs at Lake Gwendolyn (ca 8.2 cal ka BP; 8.4–8 cal ka BP) and it is possible that this time was characterised by a short-lived moisture deficit embedded within the multi-millennial phase of attenuated SWW flow at this time. This event is coincident in timing with a hydroclimatic anomaly tentatively ascribed to the 'global 8.2 cal ka event' in nearby New Zealand (Augustinus et al., 2008): a short-lived drying trend was observed at Lake Pupuke in the North Island of New Zealand at ca 8.2 cal ka BP. While suggestive, attributing this local fire event and catchment response in southwest Tasmania to the global 8.2 cal ka event requires substantial corroborating evidence from both the local and broader region.

5.3. The onset of an ENSO-influenced climate regime

A marked increase in biomass burning occurs at Lakes Gwendolyn and Nancy after ca 5 cal ka BP, with a clear shift from multi-millennial scale trends in biomass burning during the SWW dominant phase of the record to sub-millennial scale oscillations between high and low phases of biomass burning (Fig. 4). Southeast Australia (including Tasmania) falls under the influence of ENSO, with El Niño events correlated with negative moisture anomalies in this region. The increase and shift toward sub-millennial scale oscillations in biomass burning at our sites occurs in concert with a significant increase in the frequency and amplitude of El Niño events in the tropical Pacific Ocean region, from a weak ENSO signal prior to ca 5 cal ka BP to sub-millennial scale oscillations between periods of high and low El Niño frequency after this time (Fig. 4) (Moy et al., 2002; Conroy et al., 2008). While it is clear that El Niño events occurred throughout the Holocene in the tropics (Moy et al., 2002), the increase in frequency and amplitude of El Niño events post ca 5 cal ka BP appears to have allowed hydroclimatic anomalies associated with ENSO to penetrate into southwest Tasmania, an area dominated by the extra-tropical SWW system. Indeed, the increased influence of ENSO on the hydroclimate in our study area after ca 5 cal ka BP is mirrored in trends of biomass burning in other parts of ENSO climate domain, such as southern South America (Whitlock et al., 2007; Power et al., 2008; Fletcher and Moreno, 2011, 2012a). What is unclear, and requires further research, is how trends in the SWW over a range of timescales have interacted (positively or negatively) with ENSO variability to influence mid-to high latitude SH climate regimes (sensu Gomez et al., 2011). Answering this question requires coupling records from areas within (1) the ENSO domain (such as the tropical Pacific Ocean; e.g. Moy et al., 2002; Conroy et al., 2008; Yan et al., 2011), (2) the ENSO/SWW domain (such as the present study and Fletcher and Moreno, 2012b) and from within areas located in the SWW zone of influence (e.g. Moreno et al., 2014) at multiple temporal scales. It must be noted, that we cannot exclude other modes of variability (such as SAM) driving these sub-millennial scale hydroclimatic variations through this phase, although there is currently no evidence for such variations over this period.

5.4. Long-term fire regimes and catchment dynamics in southwest Tasmania

Our results show clearly synchronous trends in local and extra-local (<3 km) fire activity at two proximal study sites located on the western flank of the Frenchman's Cap massif in southwest Tasmania. Despite similarities in trends of fire activity, there are key

differences between the fire histories and catchment dynamics of the two study sites that relate to local geography. Importantly, charcoal influx at the smaller Lake Nancy is, on average, double that of the larger Lake Gwendolyn. This is despite the latter being a larger lake and having a catchment area that is an order of magnitude larger than Lake Nancy, characteristics that are usually associated with increased charcoal deposition (Whitlock and Larsen, 2001). Biomass burning and subsequent charcoal production is dependent on fuel type, condition and load (Whitlock and Larsen, 2001). The multi-millennial scale period of high fire activity and local to extra-local biomass burning between ca 11 and 8 cal ka BP is characterised by a ratio between the charcoal input into each of these lakes of 2.4:1 (Lake Nancy to Lake Gwendolyn ratio). This difference is stark, given the smaller size of Lake Nancy and its catchment relative to Lake Gwendolyn. One explanation for this difference could be a higher vegetation biomass around Lake Nancy through this prolonged dry phase (ca 11–8 cal ka BP). Higher vegetation biomass around Lake Nancy at this time is consistent with our geochemical proxies for sediment organic matter (Br and Mo Inch/Coh) and with the high organic content of soils that develop on the nutrient poor bedrock that underlies much of southwest Tasmania (Bowman et al., 1986). Fires have kept much of the lowlands of western Tasmania open for at least the last 12 cal ka (Fletcher and Thomas, 2010b) and, today, the contemporary distribution of fire-sensitive vegetation is strongly correlated with topographic protection from the prevailing SWW that fan fires across the landscape (Wood et al., 2011). The northeast aspect of Lake Nancy would have afforded its catchment some protection from fire through the multi-millennial phase of low moisture and high background burning under an attenuated SWW regime (between 11 and 8 cal ka BP), while the west-facing Lake Gwendolyn valley would not have afforded the same protection to that catchment.

The switch to lower organic content and higher detrital input into Lake Nancy after 7.2 cal ka BP marks a period of major change in the nature and type of sediment being delivered into Lake Nancy. This change occurs through the phase of lowest charcoal input for the entire ca 12 cal ka sequence at Lake Nancy, reflecting an increase in precipitation under a strengthening SWW regime. The absence of a charcoal peak coincident with this change in sediment character precludes the assumption of a high-impact fire altering catchment dynamics at this time (sensu Fletcher et al., 2014a). This transition occurs ca 800 years after a potentially fire-driven deposition of inorganic material into Lake Nancy at ca 8.2 cal ka BP. One possible explanation for the trend in sediment geochemistry is the eventual collapse of a fire-sensitive vegetation system after millennia of high fire activity both locally and in the broad region. Repeated ENSO-driven burning of rainforest over a 3 ka period drove an eventual collapse of the local rainforest and a transition to fire-promoted vegetation at a site in southern Tasmania (Fletcher et al., 2014a). This transition significantly altered the nature and type of sediment being transported from the landscape into that study lake, a transition characterised by a marked increase in the input of detrital elements (Fletcher et al., 2014a), as is seen at Lake Nancy after 7.2 cal ka BP. Despite the transition to a more variable (sub-millennial) fire regime after ca 5 cal ka BP, relative to the multi-millennial scale trends in fire activity that characterised the period between ca 12 and 8 cal ka BP (Fig. 4), the sediment geochemistry at Lake Nancy remains relatively stable (Fig. 3), suggesting that many of the local fire events were either insufficient to drive a catchment response or that they reflect fires occurring outside the small Lake Nancy catchment.

Interestingly, the sediment geochemistry of Lake Gwendolyn reveals an overall increase in organic content and a reduction in the deposition of detrital elements after 6.5 cal ka BP (Fig. 2). The westerly aspect of the Lake Gwendolyn catchment would expose this site to a higher risk of fire than Lake Nancy. The multi-millennial dry phase between ca 11 and 8 cal ka BP might have resulted in a fire frequency that precluded the formation of substantial vegetation within this catchment through this time. Increasing sedimentary organic (Br) content after ca 6.5 cal ka BP, then, possibly reflects an increase in vegetation cover at this more exposed and fire-prone site in response to increased moisture delivered by the strengthened SWW system at this time. A continuing increase in organic content at Lake Gwendolyn to the present suggests that, while local fires probably occurred within the catchment, the overall increase in moisture resulting from the strengthening SWW flow over the region was sufficient to allow increased vegetation cover in the catchment, possibly along the headwall where fire-sensitive vegetation and deeper organic soils are present today.

6. Conclusion

Here we identify a shift from multi-millennial to sub-millennial trends in fire activity at two proximal sites in southwest Tasmania after ca 5 cal ka BP, driving clear local scale catchment changes that diverged in response to local topographic and geographic factors. Southwest Tasmania lies under the influence of both the SWW and ENSO and we attribute the changes in biomass burning to changes in the relative importance of the SWW and ENSO over our study area. Fire activity in our study area between 12 and 5 cal ka BP mirrors multi-millennial scale trends in the SWW hypothesised to have occurred across the entire hemisphere at this time: decreased SWW flow and high fire activity between ca 11 and 8 cal ka BP; increased SWW flow and low fire activity between ca 7–5 cal ka BP. While not being able to discount sub-millennial scale variations in SAM (or other climate modes) over this period, we explain a shift toward sub-millennial scale trends in biomass burning at our study sites after ca 5 cal ka BP as the result of an increase in the frequency and amplitude of El Niño events in the tropical Pacific Ocean region. While ENSO variability occurs throughout the Holocene, the marked increase in ENSO variability recorded in the tropical Pacific Ocean region after ca 5 cal ka BP was sufficient for ENSO-driven climate anomalies to influence areas under the influence of the SWW. We suggest that further targeted research is required to understand how the SWW and ENSO interact to influence the climate of the mid-to high-latitudes of the Southern Hemisphere.

Acknowledgements

M.-S.F. acknowledges financial support from ARC projects DI110100019 and IN140100050, CONICYT project 3110180 and AINSE Award ALNGRA12003. Thanks for Rachael-Ann Fletcher for analysing macroscopic charcoal from TAS1106. Thanks to Scott Nichols, Jared Pedro, Lucy Gayler and Peter Shimeld for assistance in the field. We thank Agathe Lisé-Pronovost for providing the Laguna Potrok Aike magnetic data. We also thank Patricio I Moreno for valuable comments on an earlier draft of this manuscript.

References

Appleby, P., 2001. Chronostratigraphic Techniques in Recent Sediments, Tracking Environmental Change Using Lake Sediments. Springer, pp. 171–203.
Appleby, P., Oldfield, F., 1978. The calculation of lead-210 dates assuming a constant rate of supply of unsupported ^{210}Pb to the sediment. Catena 5, 1–8.
Augustinus, P., Bleakley, N., Deng, Y., Shane, P., Cochran, U., 2008. Rapid change in early Holocene environments inferred from lake Pupuke, Auckland city, New Zealand. J. Quat. Sci. 23, 435–447.
Binford, M.W., 1990. Calculation and uncertainty analysis of ^{210}Pb dates for PIRLA project lake sediment cores. J. Paleolimnol. 3, 253–267.

Blaauw, M., 2010. Methods and code for 'classical' age-modelling of radiocarbon sequences. Quat. Geochronol. 5, 512–518.
Blaauw, M., Christen, J.A., 2011. Flexible paleoclimate age-depth models using an autoregressive gamma process. Bayesian Anal. 6, 457–474.
Bowman, D.M.J.S., 1998. Tansley Review No. 101: the impact of Aboriginal landscape burning on the Australian biota. New Phytol. 140, 385–410.
Bowman, D.M.J.S., Jackson, W.D., 1981. Vegetation succession in southwest Tasmania. Search 12, 358–362.
Bowman, D.M.J.S., Maclean, A.R., Crowden, R.K., 1986. Vegetation–soil relationships in the lowlands of south-west Tasmania. Aust. J. Ecol. 11, 141–153.
Bowman, D.M.J.S., Wood, S.W., 2009. Fire driven land cover change in Australia and W.D. Jackson's theory of the fire ecology of southwest Tasmania. In: Cochrane, M.A. (Ed.), Tropical Fire Ecology: Climate Change, Land Use and Ecosystem Dynamics. Springer-Praxis, Heidelberg, pp. 87–111.
Burnett, A.P., Soreghan, M.J., Scholz, C.A., Brown, E.T., 2011. Tropical East African climate change and its relation to global climate: a record from Lake Tanganyika, Tropical East Africa, over the past 90+ kyr. Palaeogeogr. Palaeoclimatol. Palaeoecol. 303, 155–167.
Clark, J.S., Royall, P.D., 1996. Local and regional sediment charcoal evidence for fire regimes in presettlement north-eastern North America. J. Ecol. 365–382.
Conroy, J.L., Overpeck, J.T., Cole, J.E., Shanahan, T.M., Steinitz-Kannan, M., 2008. Holocene changes in eastern tropical Pacific climate inferred from a Galápagos lake sediment record. Quat. Sci. Rev. 27, 1166–1180.
Cook, E.R., Woodhouse, C.A., Eakin, C.M., Meko, D.M., Stahle, D.W., 2004. Long-term aridity changes in the western United States. Science 306, 1015–1018.
Cosgrove, R., 1999. Forty-two degrees south: the archaeology of Late Pleistocene Tasmania. J. World Prehist. 13, 357–402.
Croudace, I.W., Rindby, A., Rothwell, R.G., 2006. ITRAX: description and evaluation of a new multi-function X-ray core scanner. Special publication - Geological Society of London 267, p. 51.
Fletcher, M.-S., Moreno, P.I., 2011. Zonally symmetric changes in the strength and position of the Southern Westerlies drove atmospheric CO2 variations over the past 14 k.y. Geology 39, 419–422.
Fletcher, M.-S., Moreno, P.I., 2012a. Have the Southern Westerlies changed in a zonally symmetric manner over the last 14,000 years? A hemisphere-wide take on a controversial problem. Quat. Int. 253, 32–46.
Fletcher, M.-S., Moreno, P.I., 2012b. Vegetation, climate and fire regime changes in the Andean region of southern Chile (38° S) covaried with centennial-scale climate anomalies in the tropical Pacific over the last 1500 years. Quat. Sci. Rev. 46, 46–56.
Fletcher, M.-S., Thomas, I., 2010a. A Holocene record of sea level, vegetation, people and fire from western Tasmania, Australia. Holocene 20, 351–361.
Fletcher, M.-S., Thomas, I., 2010b. The origin and temporal development of an ancient cultural landscape. J. Biogeogr. 37, 2183–2196.
Fletcher, M.-S., Wolfe, B.B., Whitlock, C., Pompeani, D.P., Heijnis, H., Haberle, S.G., Gadd, P.S., Bowman, D.M.J.S., 2014a. The legacy of mid-Holocene fire on a Tasmanian montane landscape. J. Biogeogr. 41, 476–488.
Fletcher, M.-S., Wood, S.W., Haberle, S.G., 2014b. A fire-driven shift from forest to non-forest: evidence for alternative stable states? Ecology 95, 2504–2513.
Gadd, P., Heijnis, H., Chagué-Goff, C., Zawadzki, A., Fierro, D., Atahan, P., Croudace, I.W., Goralewski, J., 2015. ITRAX core scanner capabilities combined with other geochemical and radiochemical techniques to evaluate environmental changes in a local catchment, South Sydney, NSW, Australia. In: Croudace, I.W., Rothwell, G. (Eds.), Micro-XRF Studies of Sediment Cores. Springer, Netherlands, p. 16 (in press).
Garreaud, R.D., 2007. Precipitation and circulation covariability in the extratropics. J. Clim. 20, 4789–4797.
Garreaud, R.D., Vuille, M., Compagnucci, R., Marengo, J., 2009. Present-day South American climate. Palaeogeogr. Palaeoclimatol. Palaeoecol. 281, 180–195.
Gentilli, J., 1972. Australian Climate Patterns. The Griffin Press, Adelaide.
Gillett, N.P., Kell, T.D., Jones, P.D., 2006. Regional climate impacts of the Southern Annular Mode. Geophys. Res. Lett. 33, L23704.
Gomez, B., Carter, L., Orpin, A.R., Cobb, K.M., Page, M.J., Trustrum, N.A., Palmer, A.S., 2011. ENSO/SAM interactions during the middle and late Holocene. Holocene 22 (1), 23–30.
Hahn, A., Kliem, P., Oehlerich, M., Ohlendorf, C., Zolitschka, B., 2014. Elemental composition of the Laguna Potrok Aike sediment sequence reveals paleoclimatic changes over the past 51 ka in southern Patagonia, Argentina. J. Paleolimnol. 52, 349–366.
Harris, S., Kitchener, A., 2005. From Forest to Fjaeldmark : Descriptions of Tasmania's Vegetation. Department of Primary Industries, Water and Environment, Hobart.
Higuera, P.E., Brubaker, L.B., Anderson, P.M., Hu, F.S., Brown, T.A., 2009. Vegetation mediated the impacts of postglacial climate change on fire regimes in the south-central Brooks Range, Alaska. Ecol. Monogr. 79, 201–219.
Higuera, P.E., Gavin, D.G., Bartlein, P.J., Hallett, D.J., 2010. Peak detection in sediment–charcoal records: impacts of alternative data analysis methods on fire-history interpretations. Int. J. Wildland Fire 19, 996–1014.
Hill, K.J., Santoso, A., England, M.H., 2009. Interannual Tasmanian rainfall variability associated with large-scale climate modes. J. Clim. 22, 4383–4397.
Hogg, A.G., Hua, Q., Blackwell, P.G., Niu, M., Buck, C.E., Guilderson, T.P., Heaton, T.J., Palmer, J.G., Reimer, P.J., Reimer, R.W., 2013. SHCal13 Southern Hemisphere calibration, 0–50,000 cal yr BP. Radiocarbon 55 (4), 1889–1903.
Jackson, W.D., 1968. Fire, air, water and earth – an elemental ecology of Tasmania. Proc. Ecol. Soc. Aust. 3, 9–16.
Jackson, W.D., 1999. The Tasmanian environment. In: Reid, J.B., Hill, R.S., Brown, M.J., Hovenden, M.J. (Eds.), Vegetation of Tasmania. Australian Biological Resources Study, Canberra.
Kilian, R., Lamy, F., 2012. A review of Glacial and Holocene paleoclimate records from southernmost Patagonia (49–55°S). Quat. Sci. Rev. 53, 1–23.
Lamy, F., Kilian, R., Arz, H.W., Francois, J.P., Kaiser, J., Prange, M., Steinke, T., 2010. Holocene changes in the position and intensity of the southern westerly wind belt. Nat. Geosci. 695–699.
Lisé-Pronovost, A., St-Onge, G., Gogorza, C., Haberzettl, T., Jouve, G., Francus, P., Ohlendorf, C., Gebhardt, C., Zolitschka, B., Team, P.S., 2015. Rock-magnetic proxies of wind intensity and dust since 51,200 cal BP from lacustrine sediments of Laguna Potrok Aike, southeastern Patagonia. Earth Planet. Sci. Lett. 411, 72–86.
Liu, X., Colman, S.M., Brown, E.T., Minor, E.C., Li, H., 2013. Estimation of carbonate, total organic carbon, and biogenic silica content by FTIR and XRF techniques in lacustrine sediments. J. Paleolimnol. 50, 387–398.
Maw, G., Kempton, R., 1982. Bromine in soils and peats. Plant Soil 65, 103–109.
McCune, B., Mefford, M.J., 1999. PC-Ord for Windows, 4.27 ed. MjM Software, Gleneden Beach, OR.
McGlone, M.S., Kershaw, P., Markgraf, V., 1992. El Nino/Southern Oscillation climatic variability in Australasian and South American paleoenvironmental records. In: Diaz, H.F., Markgraf, V. (Eds.), El Nino: Historical and Paleoclimatic Aspects of the Southern Oscillation. Cambridge University Press, Cambridge.
McWethy, D., Higuera, P., Whitlock, C., Veblen, T., Bowman, D., Cary, G., Haberle, S., Keane, R., Maxwell, B., McGlone, M., 2013. A conceptual framework for predicting temperate ecosystem sensitivity to human impacts on fire regimes. Glob. Ecol. Biogeogr. 22, 900–912.
Moreno, P.I., 2000. Climate, fire, and vegetation between about 13,000 and 9200 C-14 yr BP in the Chilean lake district. Quat. Res. 54, 81–89.
Moreno, P.I., 2004. Millennial-scale climate variability in northwest Patagonia over the last 15000 yr. J. Quat. Sci. 19, 35–47.
Moreno, P.I., Vilanova, I., Villa-Martínez, R., Garreaud, R., Rojas, M., De Pol-Holz, R., 2014. Southern Annular Mode-like changes in southwestern Patagonia at centennial timescales over the last three millennia. Nat. Commun. 5.
Moy, C.M., Seltzer, G.O., Rodbell, D.T., Anderson, D.M., 2002. Variability of El Nino/Southern Oscillation activity at millennial timescales during the Holocene. Nature 420, 162–165.
Murphy, B.F., Timbal, B., 2008. A review of recent climate variability and climate change in southeastern Australia. Int. J. Climatol. 28, 859–879.
Nicholls, N., Lucas, C., 2007. Interannual variations of area burnt in Tasmanian bushfires: relationships with climate and predictability. Int. J. Wildland Fire 16, 540–546.
Phedorin, M., Goldberg, E., Grachev, M., Levina, O., Khlystov, O., Dolbnya, I., 2000. The comparison of biogenic silica, Br and Nd distributions in the sediments of Lake Baikal as proxies of changing paleoclimates of the last 480kyr. Nucl. Instrum. Methods Phys. Res. Sect. A Accel. Spectrom. Detect. Assoc. Equip. 448, 400–406.
Power, M.J., Marlon, J., Ortiz, N., Bartlein, P.J., Harrison, S.P., Mayle, F.E., Ballouche, A., Bradshaw, R.H.W., Carcaillet, C., Cordova, C., Mooney, S., Moreno, P.I., Prentice, I.C., Thonicke, K., Tinner, W., Whitlock, C., Zhang, Y., Zhao, Y., Ali, A.A., Anderson, R.S., Beer, R., Behling, H., Briles, C., Brown, K.J., Brunelle, A., Bush, M., Camill, P., Chu, G.Q., Clark, J., Colombaroli, D., Connor, S., Daniau, A.L., Daniels, M., Dodson, J., Doughty, E., Edwards, M.E., Finsinger, W., Foster, D., Frechette, J., Gaillard, M.J., Gavin, D.G., Gobet, E., Haberle, S., Hallett, D.J., Higuera, P., Hope, G., Horn, S., Inoue, J., Kaltenrieder, P., Kennedy, L., Kong, Z.C., Larsen, C., Long, C.J., Lynch, J., Lynch, E.A., McGlone, M., Meeks, S., Mensing, S., Meyer, G., Minckley, T., Mohr, J., Nelson, D.M., New, J., Newnham, R., Noti, R., Oswald, W., Pierce, J., Richard, P.J.H., Rowe, C., Goni, M.F.S., Shuman, B.N., Takahara, H., Toney, J., Turney, C., Urrego-Sanchez, D.H., Umbanhowar, C., Vandergoes, M., Vanniere, B., Vescovi, E., Walsh, M., Wang, X., Williams, N., Wilmshurst, J., Zhang, J.H., 2008. Changes in fire regimes since the Last Glacial Maximum: an assessment based on a global synthesis and analysis of charcoal data. Clim. Dyn. 30, 887–907.
Power, S., Delage, F., Chung, C., Kociuba, G., Keay, K., 2013. Robust twenty-first-century projections of El Niño and related precipitation variability. Nature 502, 541–545.
R Core Development Team, 2013. R: a Language and Environment for Statistical Computing. R Foundation for Statistical Computing, Vienna Austria.
Rees, A.B.H., Cwynar, L.C., Fletcher, M.-S., 2015. Southern Westerly Winds submit to the ENSO regime: a multiproxy paleohyrdology record from Lake Dobson, Tasmania. Quat. Sci. Rev. (submitted for publication).
Riedinger, M.A., Steinitz-Kannan, M., Last, W.M., Brenner, M., 2002. A~ 6100 14 C yr record of El Niño activity from the Galápagos Islands. J. Paleolimnol. 27, 1–7.
Rodbell, D.T., Seltzer, G.O., Anderson, D.M., Abbott, M.B., Enfield, D.B., Newman, J.H., 1999. An~ 15,000-year record of El Niño-driven alluviation in southwestern Ecuador. Science 283, 516–520.
Saez, A., Valero-Garces, B.L., Giralt, S., Moreno, A., Bao, R., Pueyo, J.J., Hernandez, A., Casas, D., 2009. Glacial to Holocene climate changes in the SE Pacific. The Raraku lake sedimentary record (Easter Island, 27 S). Quat. Sci. Rev. 28, 2743–2759.
Shulmeister, J., 1999. Australasian evidence for mid-Holocene climate change implies precessional control of Walker Circulation in the Pacific. Quat. Int. 57, 81–91.
Shulmeister, J., Lees, B.G., 1995. Pollen evidence from tropical Australia for the onset of an ENSO-dominated climate at c. 4000 BP. Holocene 5, 10–18.

Sturman, A.P., Tapper, N.J., 2006. The Weather and Climate of Australia and New Zealand. Oxford University Press, USA.
Thomas, I., Cullen, P., Fletcher, M.-S., 2010. Ecological drift or stable fire cycles in Tasmania: a resolution? In: Haberle, S., Stevenson, J., Prebble, M. (Eds.), Altered Ecologies: Fire, Climate and Human Influence on Terrestrial Landscapes. ANU E-Press, Canberra. The Australian National University.
Verdon, D.C., Kiem, A.S., Franks, S.W., 2004. Multi-decadal variability of forest fire risk-eastern Australia. Int. J. Wildland Fire 13, 165–171.
Whitlock, C., Larsen, C., 2001. Charcoal as a fire proxy. In: Smol, J.P., Birks, H.J.B., Last, W.M. (Eds.), Tracking Environmental Change Using Lake Sediments, Terrestrial, Algal, and Siliceous Indicators, vol. 3. Kluwer Academic Publishers, pp. 75–97.
Whitlock, C., Moreno, P.I., Bartlein, P., 2007. Climatic controls of Holocene fire patterns in southern South America. Quat. Res. 68, 28–36.
Wood, S.W., Bowman, D.M.J.S., 2012. Alternative stable states and the role of fire–vegetation–soil feedbacks in the temperate wilderness of southwest Tasmania. Landsc. Ecol. 1–16.
Wood, S.W., Murphy, B.P., Bowman, D.M., 2011. Firescape ecology: how topography determines the contrasting distribution of fire and rain forest in the south-west of the Tasmanian Wilderness World Heritage Area. J. Biogeogr. 38, 1807–1820.
Yan, H., Sun, L., Wang, Y., Huang, W., Qiu, S., Yang, C., 2011. A record of the Southern Oscillation Index for the past 2,000 years from precipitation proxies. Nat. Geosci. 4, 611–614.
Ziegler, M., Jilbert, T., de Lange, G.J., Lourens, L.J., Reichart, G.J., 2008. Bromine counts from XRF scanning as an estimate of the marine organic carbon content of sediment cores. Geochem. Geophys. Geosyst. 9.